Hindawi
Advances in Materials Science and Engineering
Volume 2021, Article ID 8552224, 15 pages
https://doi.org/10.1155/2021/8552224

Research Article

The Influence of Mixing Orders on the Microstructure of Artificially Prepared Sand-Clay Mixtures

Kexin Yin,[1] **Anne-Laure Fauchille**,[1] **Eugenia Di Filippo**,[1] **Khaoula Othmani**,[1] **Samuel Branchu**,[2] **Giulio Sciarra**,[1] **and Panagiotis Kotronis**[1]

[1]*Institut de Recherche en Génie Civil et Mécanique (GeM), Ecole Centrale de Nantes, UMR 6183 CNRS, 1 rue de la Noë 44321, Nantes Cedex 3, France*
[2]*Institut de Recherche en Génie Civil et Mécanique, Université de Nantes, Ecole Centrale de Nantes, UMR 6183 CNRS, 58 rue Michel Ange BP 420 44606, Saint-Nazaire, France*

Correspondence should be addressed to Kexin Yin; kexin.yin.research@gmail.com

Received 2 August 2021; Accepted 30 August 2021; Published 10 September 2021

Academic Editor: Yunzhong Jia

The mixing order of silica sand, clay (kaolinite), and water controls the microstructure of resulting artificial soil samples. Most homogeneous microstructures can be achieved by applying the mixing order "sand-water-clay." The following methods were used to validate this statement: (1) optical observation, (2) X-ray tomography, (3) scanning electron microscopy, and (4) Mercury intrusion porosimetry. For all samples, clays are mainly organized in a homogeneous matrix but are also dispersed heterogeneously in micrometer-sized layers surrounding sand particles, particularly where sand grains show a greater roughness. At water contents $\geq 1.5\, w_L$, the microstructures are visually similar from the mm to μm scale whatever mixing order is used. However, for water contents lower than 1.5 w_L, the mixing order controls the distribution of the clay particles. This paper proposes a motivated choice of a preparation protocol of artificial clayey materials to be used in laboratory experiments. It might contribute to better understanding and modeling grain movements and arrangements in artificial muds, used for instance in underground mining, foundation settlement, hydraulic containment, road construction, soil stabilization, and in natural soils in the occurrence of soil liquefaction, industrial brick manufacturing, and in studying shear processes in tectonic fault zones.

1. Introduction

Understanding the rheological behavior of soils provides insights to improve the design and long-term stability of construction foundations, roads, and artificial drilling muds. Moreover, it allows a better quantification of the risks of soil liquefaction and shrinkage and swelling disorders below civil engineering structures [1–7]. Natural soils are generally "gap-graded," i.e., classified as sandy, silty, or clayey soils based on their fine and coarse contents [8–10]. The characterization of natural soils, especially clayey soils, is very complex [11–15]. The soils can differ largely in their microstructure, which, in turn, controls their (anisotropic) petrophysical properties and their rheological behavior.

Reconstituted or artificial soils with similar fabric to natural soils are widely used in laboratory testing [16–18]. In particular, sand-clay mixtures are commonly employed as simplified and reconstituted soils in the laboratory to investigate the thermo-hydro-mechanical behavior of clayey soils [13, 19–27]. The macroscopic behavior of soils is usually known to be controlled by the microstructure, which was examined by several studies [28–31]. Yet, a very significant number of studies on the thermo-hydro-mechanical behavior of sand-clay and clay-clay mixtures [32–37] produced their samples in differing ways and potentially ignored the effect of different microstructures induced by sample preparation that might have altered the experiments outcomes. The verification of the microstructure after the preparation is rarely known, except for classical material characterization. For example, Vallejo and Mawby [21] prepared dry sand-clay mixtures by shaking samples in sealed plastic bags until visual homogeneity; Polidori [38] by

adding deionized water into the mixture, the mixture was then placed in an oven at 60°C to eliminate humidity absorbed from the atmosphere before being mixed; Bendahmane et al. [39] and Marot et al. [40] mixed sand and water at a water content of 8% for three minutes and clay powder was then added progressively during mixing.

The preparation of reconstituted clayey soils should require as much fabric homogeneity (i.e., uniformity) as possible to allow for a high number of identical test repeats [13, 16, 41]. Otherwise, the micromechanical behavior of soil at small scale, which takes into account the variability of the heterogeneities, can result in different macroscopic behavior and potentially identify the characteristics of a representative volume element [42, 43].

This study investigates the microstructures that result from three different mixing protocols of silica sand, clay, and water. For that, optical observation, 3D X-ray tomography, 2D scanning electron microscopy (SEM), 2D environmental scanning electron microscopy (ESEM) images, and Mercury intrusion porosimetry (MIP) analyses were carried out on wet and dry samples.

The paper is organized as follows: Section 2 is devoted to the characterization of the primary materials used; Section 3 describes the sample preparation and the methods used to investigate the microstructure; Section 4 presents the results and, finally, Section 5 discusses and concludes these findings.

2. Materials

The materials used in this research are presented in this section. Fontainebleau sand, clay, and distilled water are used to prepare the sand-clay mixtures in the laboratory.

2.1. Fontainebleau Sand. Fontainebleau sand NE34 (called hereafter FSand NE34) from Sibelco company (France) was used to prepare sand-clay mixture samples. Fontainebleau sand is fine siliceous sand, which is widely utilized as reference material in many experimental studies [6, 7, 44–49]. Energy dispersive spectrometer (EDS) analyses show that FSand NE34 is composed of 99% quartz (SiO_2). Table 1 illustrates the solid matter density and characteristics of the grain size distribution. In the secondary electron (SE) images, FSand NE34 shows both angular and smooth particles with a heterogeneous roughness (Figures 1(a) and 1(b)).

The grain size distribution of FSand NE34 is given in Figure 2(a), which was gained by laser granulometry test and corresponds to the literature values [46, 48]. There are no grains larger than 300 μm, according to the test results.

2.2. Clay. An industrial kaolinite-rich clay material (called hereafter K Clay) from Argeco company (France) was chosen to prepare the sand-clay mixtures, in agreement with previous studies [24, 38, 50–52]. The kaolinite-rich clay material used corresponds to the material K3 in San Nicolas et al. [51]. Based on XRD data from Aboulayt et al. [53] and San Nicolas et al. [51], it contains 55% of pure kaolinite. For the composition of the clay, we refer to San Nicolas et al. [51] as well.

Table 1: Physical parameters of FSand NE 34 and K Clay.

Materials	ρ_s (g/cm^3)	d_{10} (μm)	d_{50} (μm)	$C_u = d_{60}/d_{10}$ (−)
FSand NE34	2.65	136	210	1.70
K clay	2.63	4.23	47.53	15.07
K clay dispersed	2.63	1.37	8.56	9.51

Kaolinites are present as micrometer-sized individual particles and multimicrometer aggregates (Figure 1(d)). The main parameters of K Clay are summarized in Tables 1 and 2. Note that the gained liquid (w_L) and plastic limits (w_p) of K Clay correspond to literature values, in particular to soils significantly rich in clays [35, 54, 55].

The grain size distribution of the K Clay has been obtained by two laser granulometers with three runs each: (1) by using a dispersed K Clay in distilled water in order to characterize the classical distribution of the material, and (2) by using a dry K Clay powder, which is not dispersed (Figure 2(a)). The particle size distribution of the aggregates already present in the dry material (which will be mixed with sand and water afterward, see Figures 3 and 4) is quantified.

The characterization obtained for the two types of samples is given in Table 1. When not dispersed in distilled water, K Clay shows a mean grain size d_{50} by a factor of 5.5 higher than that relative to water dispersed K Clay. The diameter of the aggregates is from 1 μm to 100 μm (Figures 2(a) and 2(b)). SEM images show that those aggregates are composed of clays or small grains of quartz surrounded by clays (Figures 1(c) and 1(d)).

3. Methods

The following paragraphs describe sample preparation and analytical methods used in this research.

3.1. Sample Preparation. Three different mixing orders of dry FSand N34, dry K Clay and distilled water were performed (Figure 3). Each mix was composed of 50 wt.% K Clay (100 g) and 50 wt.% FSand NE34 (100 g). Liquid and plastic limits of the mixture were $w_L = 22.4\%$ and $w_p = 13.7\%$, respectively (obtained by the Casagrande apparatus). Water was added in different quantities. In total, seven moistened samples were prepared for three different mixing orders, as detailed in the following, yielding pastes of 0.5, 1.0, 1.25, 1.5, 1.75 to 2.0 times the liquid limits. All samples were mixed by rotating a stirring glass stick in a container (1000 mL) for 10 minutes [39, 40] until visual homogenization and to limit air drying. The three protocols were as follows (Figure 3):

(S1) Samples were mixed by sand, then water, then clay. In samples S1, clay was added progressively in sand water mixture, by steps of 5 to 10 g and mixed for 1 min.

(S2) Samples were mixed by sand, then clay, then water. In samples S2, water was added to the dry sand-clay

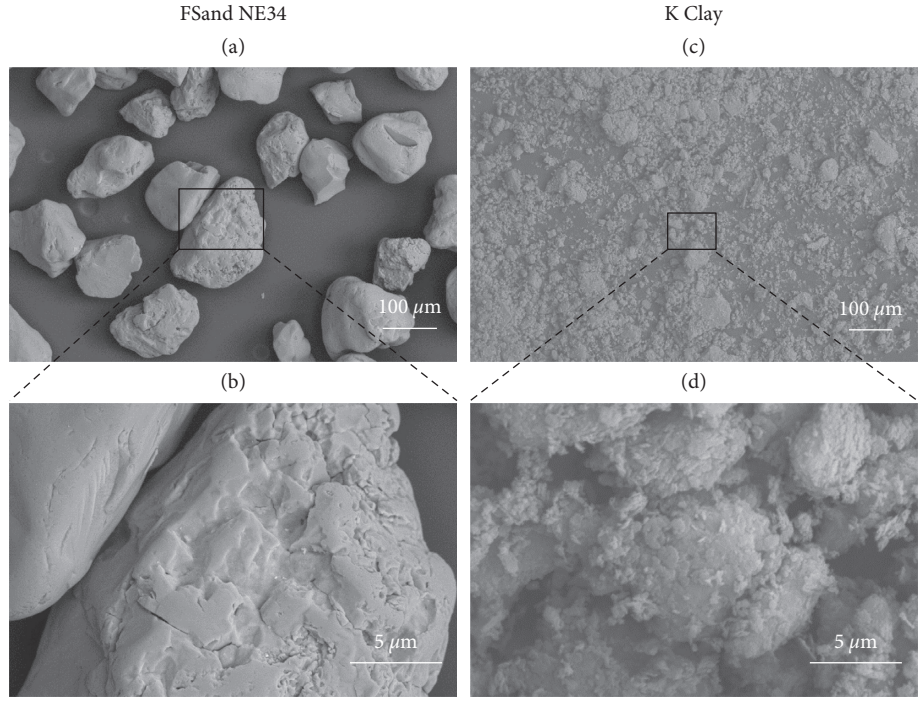

Figure 1: Secondary electron (SE) images under SEM of (a) low magnification view of FSand NE34; (b) high magnification view of FSand NE34; (c) low magnification view of K Clay; (d) high magnification view of aggregates in K Clay.

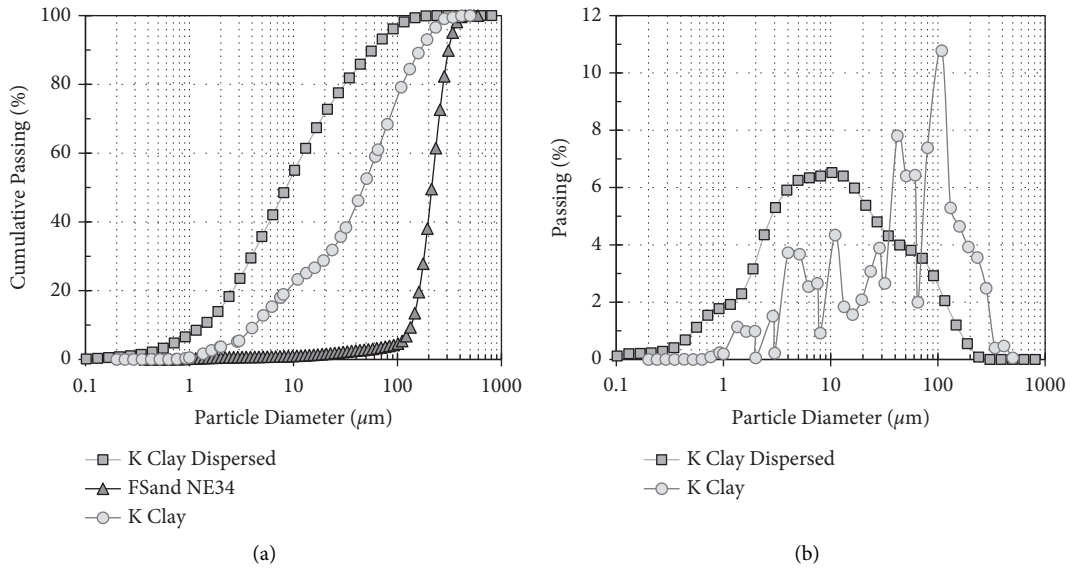

Figure 2: (a) Grain size distribution of FSand NE34 and K Clay represented by the cumulative passing as a function of particle diameter; (b) Passing fraction as a function of particle diameter for the K Clay dispersed and nondispersed.

Table 2: Characteristics of K clay from Argeco.

Clay purity (wt.%)	Liquid limit (%)	Plastic limit (%)	Plasticity index (–)	ρ_s (g/cm^3)
55	37.3	19.0	18.3	2.63

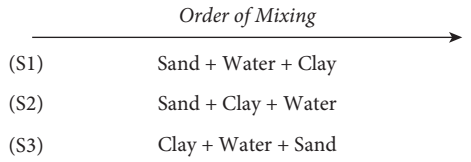

Figure 3: The three protocols for mixing sand, clay, and water.

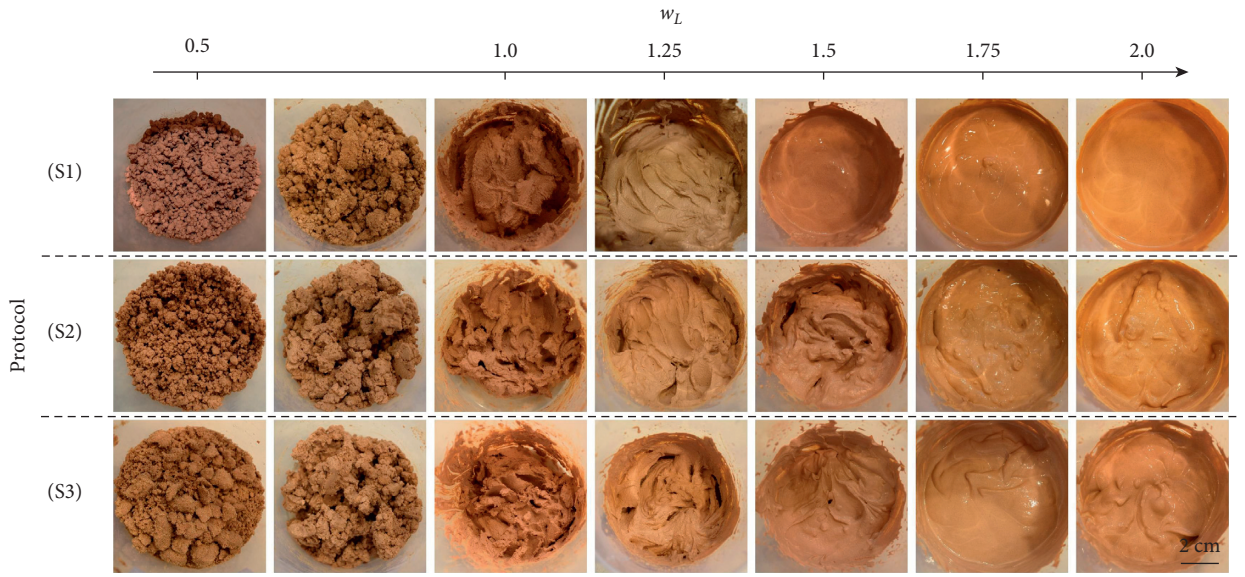

Figure 4: Optical images of the macrostructure of the sand-clay mixtures at water contents from 0.5 to 2.0 w_L.

mixture with a spray in order to ensure its homogeneous distribution [56].

(S3) Samples were mixed by clay, then water, then sand. In samples S3, sand was added progressively to clay water mixture by steps of 5 to 10 g.

After mixing, the samples were placed in a vacuum device [17, 57] for 1 hour to remove potential air bubbles. The samples were then oven-dried (48 hours at 105°C) for microstructure analyses, as X-ray tomography, scanning electron microscopy, and Mercury porosimetry measurements require dry samples [58–60]. The samples were firstly oven-dried to obtain dry samples for the microstructure observation to make sure that there is no structural change during observation and no damage on the device (e.g., the electronic column). The samples were then cut by hand to get a fresh surface, without any polishing or disturbing handling on it. This subsampling technique can minimize the microstructure disturbance and prevent possible artefacts due to the subsampling process.

Referring to the concept of the smallest representative elementary area (REA) of the phase fraction in a sample, clearly explained in Houben et al. [61], the size of the sand-clay mixture samples for SEM scanning was chosen to be about 10 mm × 10 mm, which is much larger than the mean grain size of the sand. This choice is a compromise between observing the largest surface as possible and avoiding a too large sample in the SEM chamber. Conversely, bigger samples were used for X-ray tomography and MIP analyses. The choice of sample size for X-ray tomography was driven by the need for an adapted resolution to distinguish the sand and the clay matrix: cylindrical samples of 4 mm in diameter were adopted to be representative of the phase fraction of the entire sample. Moreover, the recommendation for the MIP analyzer in our lab was to consider a volume of $1 \times 1 \times 1\ cm^3$.

Besides, humid samples were prepared just before observation under environmental scanning electron microscopy to compare humid with dry microstructures. A total of 36 samples was prepared.

3.2. Analytical Methods

3.2.1. Scanning Electron Microscopy (SEM). SEM is commonly used in geosciences to investigate the microstructure of clay materials [27, 54, 62–65]. A secondary electron (SE) signal was used to acquire electronic images of the surface of samples. Before observation, the specimens were gold-coated to ensure electron reflection and interactions on their surface. The acquisition was performed in a JEOL JSM-6060 LA, at a voltage of 20 kV and at magnifications between ×40 and ×20000, in high vacuum secondary electron (SE) imaging and low vacuum backscattered electron (BSE) modes. SEM observations of microstructures were carried out on 8 different areas from each scanned sample to ensure the representative elementary area of the whole sample [61, 66]. The SEM tests were conducted on the mixtures with an initial water content of 0.5, 1.0, and 1.5 w_L, to investigate different microstructures for the same protocol.

3.2.2. Environmental Scanning Electron Microscopy (ESEM). ESEM allows the examination of specimens' surfaces in either wet or dry conditions, under insulating or conducting conditions [67].

Three humid samples from S1, S2, and S3 procedures were prepared at 1.5 w_L and placed in the ESEM chamber. Pressure and temperature conditions were kept constant during the observations. Investigations were conducted in a Zeiss EVO® 40 using a pressure of 946 Pa, at a temperature of 20°C, a voltage of 20 kV, and relative humidity between 88 and 42%. Backscattered electron (BSE) mode was used with a working distance of 5.5 mm. In total, 9 areas of each sample were scanned at different magnifications.

3.2.3. X-Ray Tomography. X-ray tomography has been shown to be very powerful in recording the multiscale microstructure of materials in 3D, even in 4D (i.e., 3D plus time). Although small clay particles and pores are commonly below its resolution limit [68–77], the distribution of sand grains in the sand-clay mixtures can be imaged.

For this, X-ray tomography scans of the dry samples were acquired with an XRadia Micro XCT-400 device, spending 9 hours recording time on each sample, yielding the acquisition of 1800 projections. The resolution was 2.3 μm/pixel, and the diameter of imaged samples was about 4 mm. The sample diameter has been chosen in such a way that, because of the usual 1000 ratio between the size of the sample and the expected resolution (μm·pixel^{-1}), the last could be of the order of few μm. This allowed detecting the different phases of the mixture, i.e., sandy grains, clay matrix, and macroporosity, separately. Each sample was placed into a thin kapton tube with an inner diameter of 4 mm to ensure sample stability during scanning.

After the reconstruction of raw images, the grey level (8 bit) volumes were filtered by a 3D median filter in ImageJ software ($2 \times 2 \times 2$ voxels), followed by a nonlocal mean filter [73, 78]. The 3D segmentation was set on volumes of $852 \times 823 \times 1000$ voxels for each. The volume data from reconstructed images were then segmented in macroporosity, sand and clay matrix components by ImageJ to quantitatively investigate the differences in the three preparations. The segmentation threshold of macroporosity, FSand NE34, and K Clay was defined by using the histogram of grey levels with well distinct peaks over the stack of images [58, 64, 79]. Only particles larger than 10 voxels were considered in this study [64] to avoid any resolution artefacts. The volume fraction of each phase was finally calculated by the analysis tool pack in ImageJ.

3.2.4. Mercury Intrusion Porosimetry (MIP). Mercury intrusion porosimetry (MIP) is a technique usually applied for the characterization of connected porous networks. It is a standard and effective method employed for measuring macro-, meso-, and micropore size distributions of a large range of materials, such as concrete, rocks, and soils [35, 80–83].

The Washburn equation relates entry pressure and pore diameter (Eq. (1) and can be applied to estimate the diameter of pore throat intruded at each pressuring step during the MIP test [80, 81, 84, 85]:

$$d = \frac{-4\gamma \cos\theta}{P}, \quad (1)$$

where d is the diameter of the pores being intruded, γ is the surface tension of Mercury, θ is the contact angle of Mercury on the soil, and P is the applied Mercury pressure.

Mercury intrusion porosimetry (MIP) was used to quantify the pore size distribution of three dry sand-clay samples prepared by the three mixing protocols, having an initial water content of 1.5 w_L. Cubic specimens of 1 cm^3 were carefully cut from each preparation to serve the Mercury intrusion porosimetry (MIP) experiments. The tests were repeated two times for each sample preparation protocol. The MIP was carried out in an AutoPore IV 9500 V1.05 device with low- and high-pressure modes. The measurement range of low pressure was 0~345 kPa, with a resolution of 69 Pa, transducer accuracy was ±1% of full scale (from transducer manufacturer's specifications). Test under low-pressure mode allowed the detection of the pore diameter size ranging from 360 to 3.6 μm. The range of high-pressure measurement was from 101 kPa to 228 MPa. Pressure resolution was 689 Pa from 101 kPa to 21000 kPa, and 1400 Pa for pressure from 21000 kPa to 228 MPa. The test under high-pressure mode allowed the detection of pore diameter size ranging from 6 to 0.005 μm, with a full-scale transducer accuracy of ±0.1%.

It is worth noting that, in general, 0.001 μm is the lattice distance of most clays, i.e., at that resolution all is void space with some supertiny neutrons, protons, and electrons.

3.2.5. Geotechnical Tests. The mechanical behavior of the sand-clay mixtures prepared according to the three protocols was investigated by performing classical one-dimensional oedometer and direct shear tests. The sand-clay mixture samples for both the oedometer and direct shear tests were prepared at 50% K Clay content and mixed with an initial water content of 1.5 w_L. The loading steps of the effective vertical stress were 12.5 kPa, 25 kPa, 50 kPa, 100 kPa, 200 kPa, 400 kPa, 800 kPa, then unloaded to 50 kPa. The direct shear tests were carried out with a normal stress of 100 kPa and a shear rate of 0.006 mm/min. The shear box was installed in a container (see [7, 18, 48]) that was filled with distilled water to guarantee a saturated specimen. The samples were performed with a displacement-controlled shearing until a maximum horizontal displacement of 5 mm (i.e., constant volume state). The shearing rate (i.e., 0.006 mm/min) was small enough to ensure a drained shearing. It was chosen in accordance with ASTM-D3080 [86] to guarantee that excess pore water pressure was dissipated during the shearing process.

4. Results

The analytical results of multiscales (from macro- to micro-) are presented hereafter, aiming to find an optimum initial mixing water content and assess the uniformity of samples reconstituted by the three sample preparations.

4.1. Macrostructures of Sand-Clay Mixtures at Different Water Contents. Photographs of the samples during mixing are shown at different initial water contents (0.5, 1.0, 1.25, 1.5, 1.75, and 2.0 times of w_L) in Figure 4 for the three protocols S1, S2, and S3.

At a water content of 0.5 times of w_L, millimeters to centimeters size aggregates are formed during the mixing process in S1 and S2 samples, while in S3, most of the aggregates are multi centimeter-size. Between 0.5 w_L and 1.0 w_L (but not exactly at 0.75 w_L), all samples contain multimillimeter size aggregates, with sand and clay heterogeneously distributed in the mixtures. At $w = 1.0$ w_L and $w = 1.25$ w_L, aggregates are progressively diluted within the mixtures. At 1.5 w_L, S1 samples resemble a visually homogeneous paste, contrary to S2 and S3 samples, which still contain macroscopic aggregates. At 1.75 w_L and 2.0 w_L, samples prepared by S2 and S3 still contain a few macroscopic aggregates, contrary to S1. At 2.0 w_L, the sand starts to sediment by using S1 protocol and sandy grains are separated from clay particles.

At the same water content and same weight fraction of sand and clay, the macrostructure of the samples (in terms of volume and size of aggregates) depends on the sample preparation. S1 at 1.5 w_L is the first configuration to be visually homogeneous among all samples and water contents tested.

4.2. 2D Microstructures of Dried Samples. After mixing, all the samples were placed into the oven (48 h at 105°C). Subsequently, surfaces of samples prepared by S1, S2, and S3 protocols and at initial water contents of 0.5, 1.0, and 1.5 w_L were selected and compared using SEM. The goal of the observation is double: (a) to choose the most suitable initial water content to get a uniform microstructure of the mixture, and (b) to identify differences and similarities of microstructures between the protocols at the most suitable water content (Figure 5).

With S1-type samples, the clay forms a somewhat continuous thin film around sand grains, while in S2 and S3 samples, sand grains are only partially covered by clays (Figure 5). The continuity of the clay film after desiccation shrinkage in S1 prepared samples suggests a more homogeneous distribution of clay particles within the samples.

The cut sample surfaces show cracks and voids, preferentially at sand grain boundaries but also between clay particles. In all samples, clay is present as a clay matrix between sandy grains and by a heterogeneous and orientated micrometer-size clay layer around sandy particles. Some sandy grains are also not covered by clay, especially in S3 but also in S2 and S1 samples initially prepared at 1.5 w_L. Notice that in S1, the sand looks more homogeneously covered by clays, but the thickness of the clay covering among all samples, during mixing and or due to desiccation, can not be quantified.

In general, SEM analyses support the conclusion from photography (Figure 4), in such that (a) S1-type samples are the most homogeneous at initial water content ≤ 1.0 w_L conditions and (b) at initial water content equal to 1.5 w_L all mixing orders yield homogeneous pastes.

For general laboratory engineering applications, only homogeneous samples should be considered, so the water content was fixed at 1.5 w_L for sample mixing in the rest of the manuscript.

4.3. 2D Microstructures of Wet Sand-Clay Mixtures at 1.5 w_L. Low and high magnification images of the humid samples' surfaces were acquired by ESEM observations (i.e., Figure 6). As previously observed under SEM in dry conditions, S1 samples show a higher continuity of the clay matrix, characterized, for example, by clay bridges between grains, compared to S2 and S3, which contain a significant number of voids between sandy grains (see Figures 6(a)–6(c)). Large sandy grains are covered or partially covered by clay particles mixed with small sandy grains and micrometer-sized clay aggregates (Figures 6(d)–6(f)). All samples show the absence of clay particles on the sharp sand edges (Figures 6(g)–6(h)).

Comparing images of pure sand (Figures 1(a) and 1(b)) with those of sand-clay mixture, it is clear that clay covers the surface of sandy grains with a minimum roughness (Figure 6(f)). Sharp edges are not covered by clay; this suggests a roughness threshold for clay covering that might be specific for each mixing order. Clay is therefore heterogeneously distributed on the surface of sandy grains (Figures 6(f) and 6(g)) due to two effects: the heterogeneous roughness of sand surface (Figures 1(a) and 1(b)) facilitates local accumulations of humid clay particles around sand during mixing, and the round shape of sand facilitates the covering of clay particles (in a thin layer) during particle rolling in the mixing process. The effect of sand geometry on clay arrangement is therefore investigated below.

4.4. 3D Mesostructure of Sand-Clay Mixtures at 1.5 w_L. In all samples, macroporosity is composed of macropores and cracks at sand-clay interfaces and in the clay matrix (Figures 7(a)–7(c) in black).

An example of macroporosity, sand and clay segmentation is given in Figure 7(d). The volume fractions resulting from the phase segmentation are shown in Table 3. Due to the resolution of image acquisition of X-ray tomography, only particles above 10 voxels can be observed and segmented. Therefore, just particles above 121.7 μm^3 are taken into account, which corresponds to a mean diameter of 6.2 μm for spherical particles.

The mean macroporosity detected in S1, S2, and S3 is slightly the same at 10.02% on average with a ±0.7% fluctuation (Table 3). Considering a dry density of K Clay of 2.63 g·cm^{-3} and FSand NE34 of 2.65 g·cm^{-3}, weight fractions were calculated from the volume fractions. K Clay and FSand NE34 represent 44.0 and 56.0% for S1, 43.4 and 56.6% for S2, and 42.8 and 57.2% for S3. The initial weight fractions of FSand NE34 and K Clay are 50% each, so the difference of fractions after drying is attributed by the surplus of 6 to 7.2% of small grains of quartz in the K Clay, significantly larger (>6.2 μm in diameter) to be segmented by image analysis.

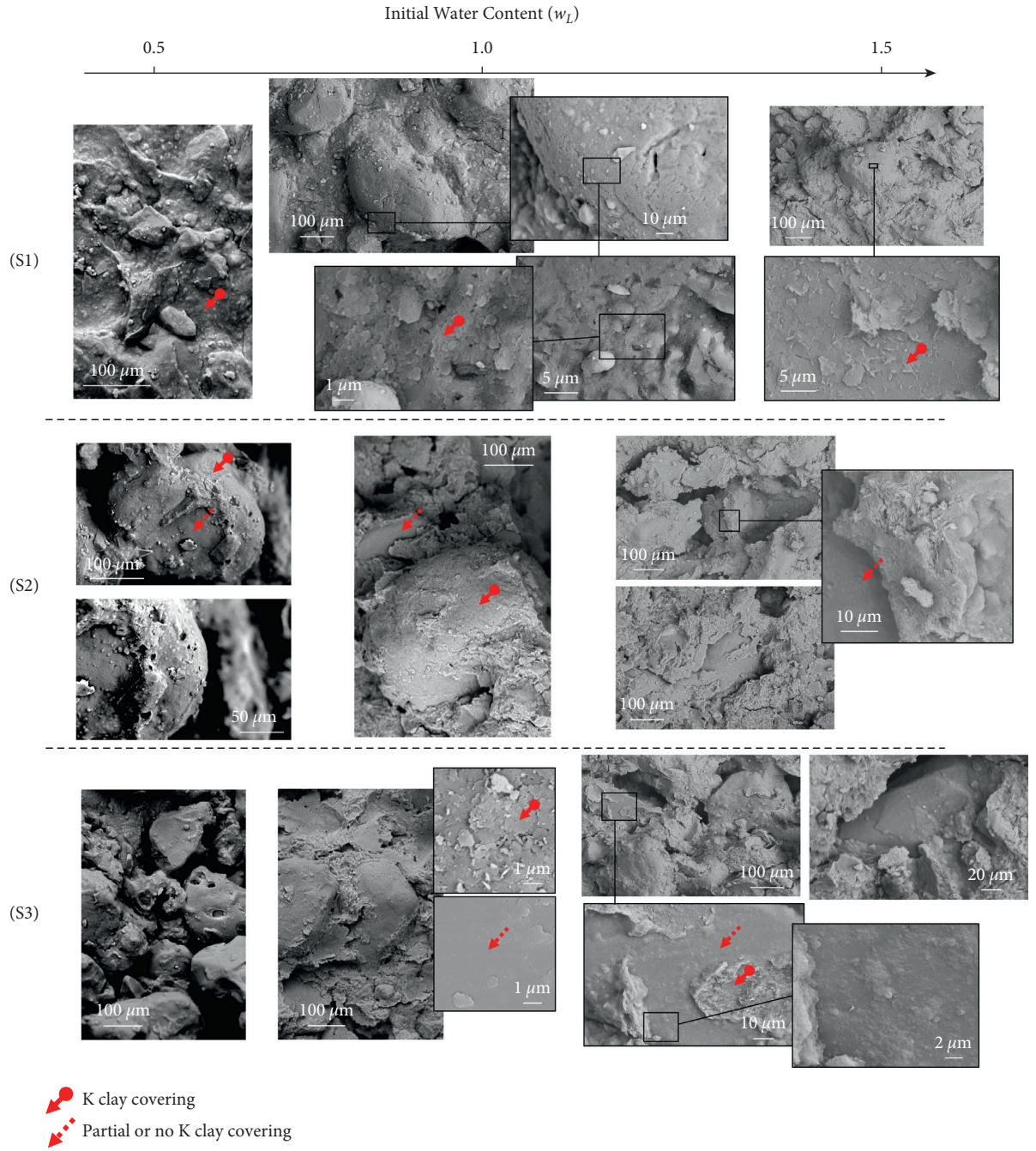

FIGURE 5: SEM images in secondary electron imaging mode of samples prepared by the three protocols in dry conditions and mixed at different initial water contents.

The normalized frequency of macropore and crack volume is compared for the three samples in Figure 7(e). Each distribution is fitted by a power law. According to coefficients of the fitting power laws and the raw images, the size distributions of macropores and cracks within the samples is very close and no significant difference is recorded.

The mean macroporosity and the macroporosity distribution are similar within the samples and no influence of sample preparation is detected in 3D under X-ray tomography at the resolution used.

4.5. MIP on Dry Sand-Clay Mixtures Initially Prepared at 1.5 w_L. MIP tests were carried out on dry samples, prepared initially at 1.5 w_L by the three protocols. The presence of microporosity, mesoporosity, and macroporosity is detected by three peaks in the pore volume distribution curve (Figure 8), as usual for clay soils.

Pore throat diameters (d_p) are classified into six scale categories based on pore diameter values [83, 87–89]:

(i) Optical pores of $d_p > 100000$ nm, including cracks in the mixture

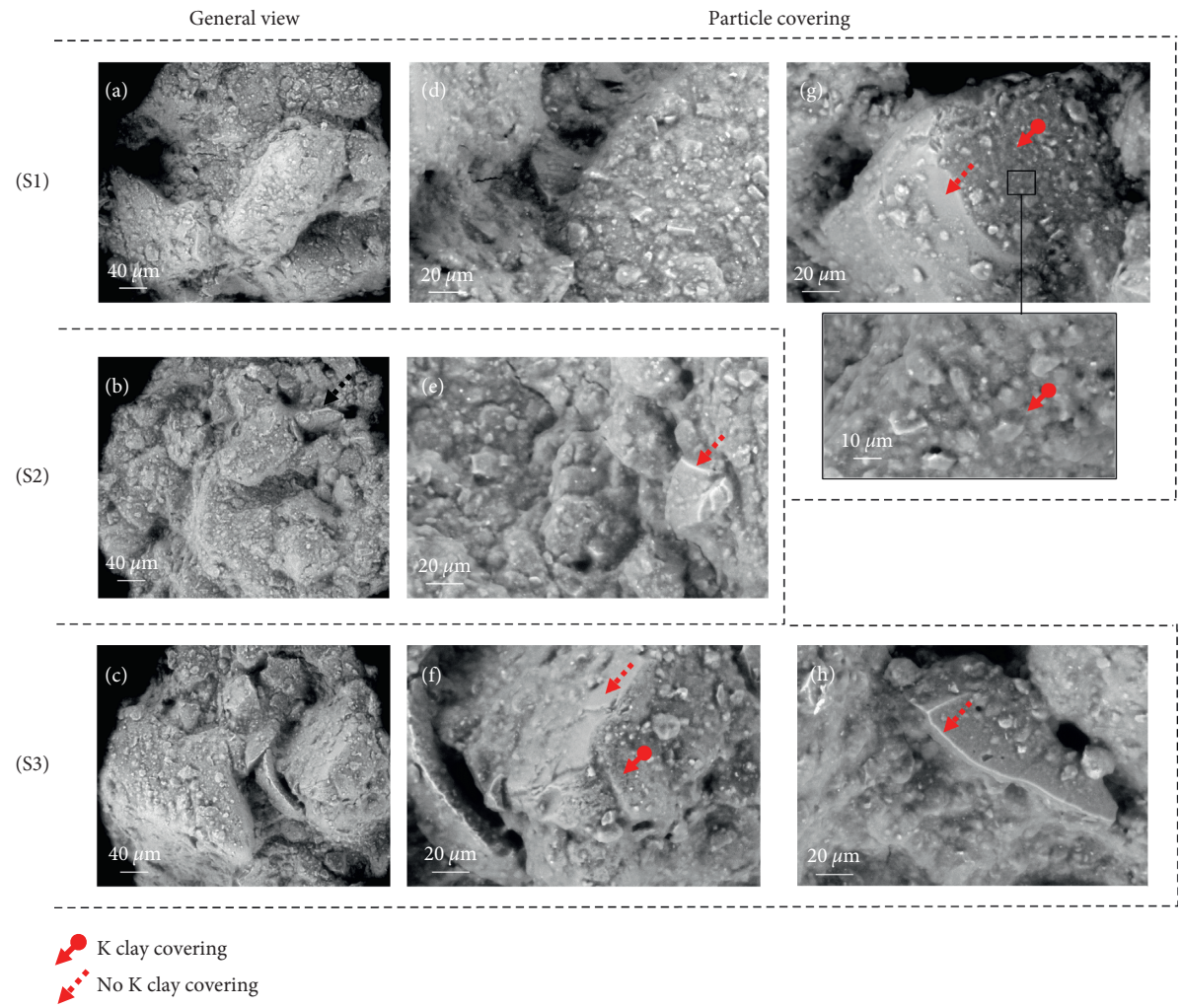

Figure 6: Low magnification views under ESEM of humid (a) S1, (b) S2, (c) S3 samples; high magnifications views of sandy grain boundaries and clay matrix of (d) S1, (e) S2, (f) S3 samples; (g) detailed views of sand boundaries of S1 sample and (h) sand arete in S3 sample.

(ii) Large-size pores of $10000 < d_p < 100000$ nm, mainly cracks and pores between clayey and clay-sand aggregates (macropores)

(iii) Medium-size pores of $5000\,\text{nm} < d_p < 10000$ nm, mainly the ones within the clayey aggregates (mesopores)

(iv) Small-size pores of $400\,\text{nm} < d_p < 5000$ nm, mainly between clay particles and partly within the aggregates (also treat as mesopores)

(v) Micropores of $10\,\text{nm} < d_p < 400$ nm, between clay particles

(vi) Ultra-micropores of $d_p < 10$ nm, mostly the ones inside clay particles

Macroporosity is composed of optical pores and macropores (i + ii), mesoporosity of medium and small-size pores (iii + iv) and microporosity of micropores and ultramicropores (v + vi) (Figure 8). The distributions of the porous volume are qualitatively superimposed for the microporosity and mesoporosity of S2 and S3 (Figure 8). S1 shows a significantly different distribution, in particular for mesoporosity, which is detected at larger pore throat diameters than S2 and S3. The distributions of macroporosity volume are all different among the sample preparations and attributed to various connectivity of cracks.

Quantitative values of mean porosity and mean and median pore throat diameter are deduced from the analysis of the pore volume distribution and the cumulative Mercury intrusion curves (Tables 4 and 5; Figure 9). Mean porosity values are 28.1% for S1, 30.1% for S2, and 28.6% for S3 (Table 4; triangles in Figure 9), with a maximum difference of around 2%. S1 samples have smaller average and median pore diameters than S2 and S3 (see Table 4), indicating S1 samples are less porous (in terms of connected porosity) than the other two. This result is confirmed by Tables 5 and 6, which shows the different volume fractions of macroporosity, mesoporosity, and microporosity according to the preparation protocol and the mean pore throat size as a function of the porosity category. Mesopores can be found commonly within clay aggregates (pores iii + iv). As S1-type samples contain fewer clay aggregates than S2 and S3, it also shows

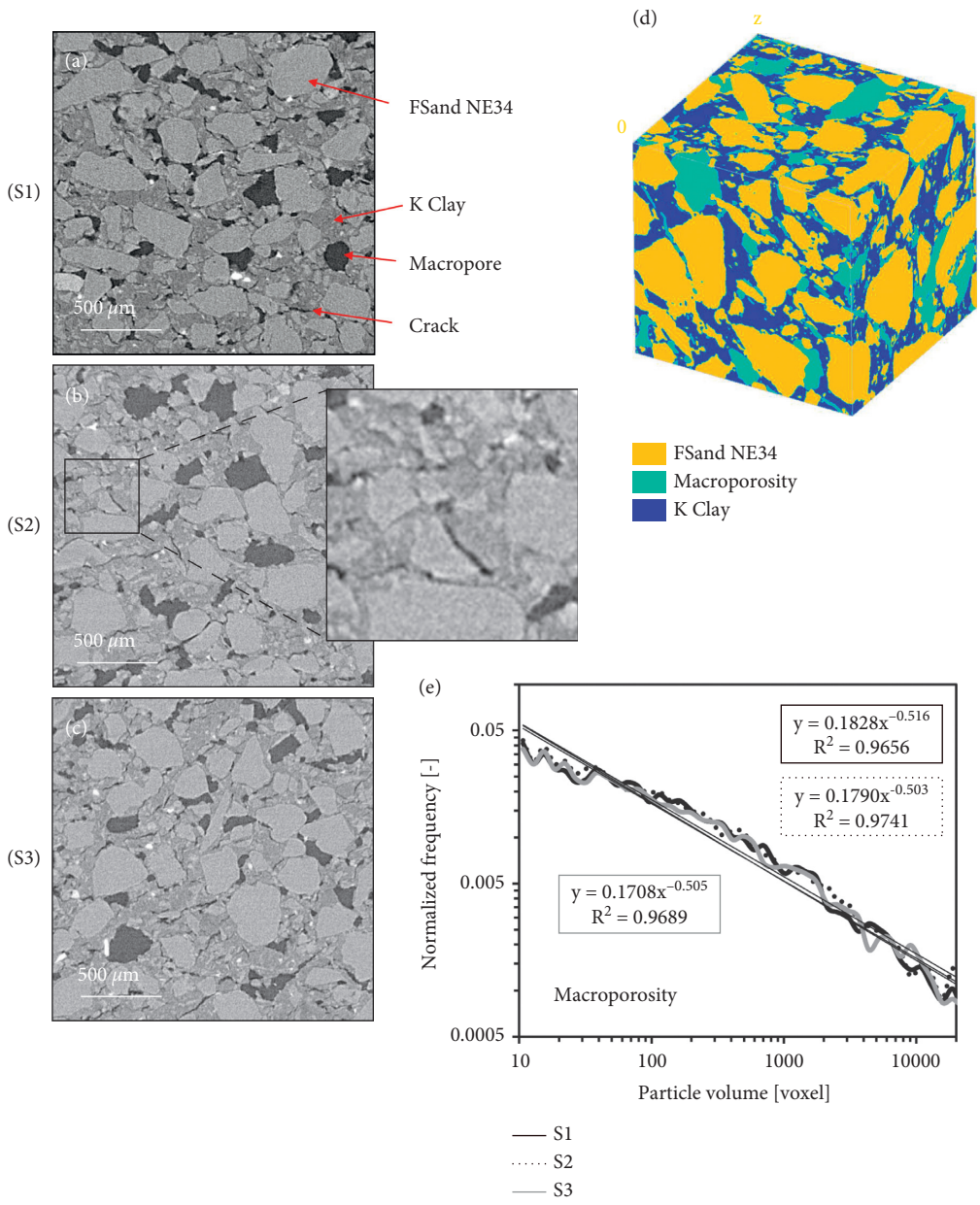

Figure 7: Mesostructures of (a) S1, (b) S2, (c) S3 samples under X-ray tomography; (d) image segmentation of FSand NE34, K Clay and macroporosity in an extract of an S3 sample; (e) macropore size distribution for the three samples prepared initially at 1.5 w_L and after drying at 105°C.

Table 3: Comparison of the volume fractions (%) of the three samples.

Sample	Macroporosity (%)	K clay (%)	FSand NE34 (%)
S1	10.44	39.60	49.96
S2	9.39	39.51	51.10
S3	10.22	38.56	51.22

fewer mesopores. However, the aggregates are larger and can hence accommodate larger mesopores.

In other words, the sample preparations change the balance of volume fractions of connected macroporosity, mesoporosity, and microporosity for the samples investigated. These changes sum up to a maximum of only 5% variation of the entire pore volume. This variation is mainly due to different macropore sizes (56% pore diameter variation), while meso- and micropores contribute much less to this discrepancy (10% and 5.8% pore diameter variation, respectively).

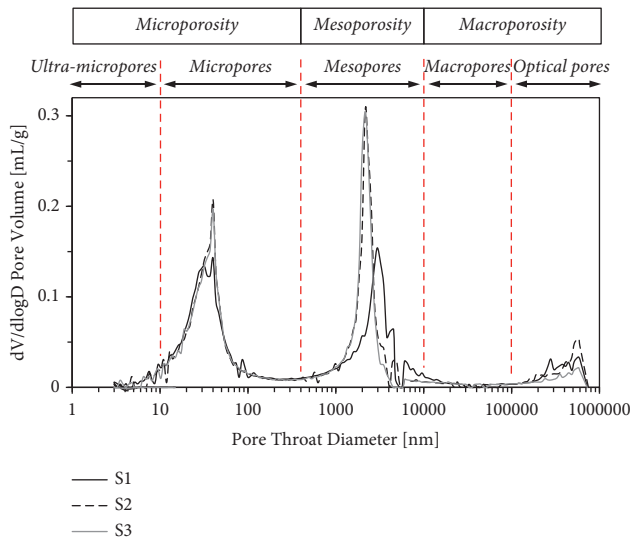

Figure 8: Pore throat diameter distribution for the samples prepared by the three protocols.

Table 4: Porosity and pore throat diameters from the MIP tests for the samples prepared by the three protocols.

Sample	Porosity (%)	Average pore diameter (4 V/A) (nm)	Median pore diameter (V) (nm)
S1	28.1	51.4	360.9
S2	30.1	58.4	1041.3
S3	28.6	54.6	480.7

Table 5: The pore volume fraction from the MIP tests for the samples prepared by the three protocols.

Sample	Optical pores (%)	Macropores (%)	Mesopores (%)	Micropores (%)	Ultramicropores (%)
S1	9.69	3.03	37.05	47.82	2.41
S2	10.42	2.38	40.55	44.79	1.86
S3	5.55	2.61	42.35	47.29	2.20

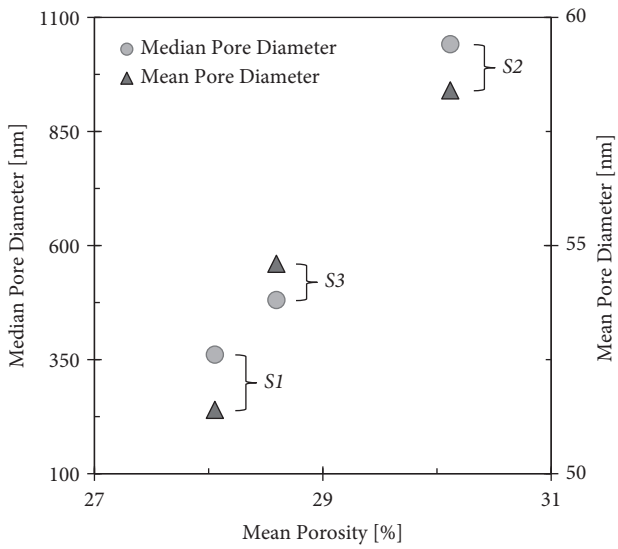

Figure 9: Median and mean pore size as a function of the mean porosity for samples prepared by S1, S2, and S3 protocols.

Table 6: Mean and median pore throat diameters from the MIP test.

	Sample	Optical + macropores	Mesoporosity	Microporosity + ultramicroporosity
Mean pore diameter (nm)	S1	70422.93	1992.71	25.98
	S2	98532.90	1878.81	27.49
	S3	63111.83	1802.53	27.28
Median pore diameter (V) (nm)	S1	314548.48	2854.54	29.58
	S2	414553.75	2243.98	35.78
	S3	260737.75	2169.59	34.43

4.6. Mechanical Behavior in Geotechnical Tests. The mechanical response of the three sample preparations, from oedometer and direct shear tests, is presented in Figure 10. The mechanical behavior of soils is usually largely dependent on the changes in microstructure that occur at the particle level [54, 62]. It can be observed that the mechanical behavior of the samples is quite close; i.e., the macroresponse is not influenced by the microscopic heterogeneities. In other words, at 1.5 w_L, the sand-clay mixture samples prepared with the S1, S2, and S3 protocols are sufficiently homogeneous at the macroscopic scale to show a similar repeatable mechanical behavior in oedometer and direct shear experiments, whatever the sample preparation is.

5. Discussion

A comprehensive discussion based on the results mentioned above is presented as follows.

5.1. Flocculation and Aggregation during Mixing. At the macroscale, the three types of samples contain various sizes of aggregates despite of identical fractions. Flocculation and aggregation are linked to the adsorption of water on the clay particle surfaces [90]. S1 protocol consists of mixing sand and water, then clay progressively. Contrary to other mixing orders, water is therefore fully accessible to the clay fraction, even at water contents lower than 1.5 w_L. The charged surface of clay particles can adsorb water, which allows individual particles to form aggregates [91]. Due to the significant excess of water in the mixture and continuous stirring, those flakes are directly diluted, as flocculation is a reversible process [92]. In the other cases (S2 and S3), clay is the majority phase compared to water. Kaolinite adsorbs water at each water addition and clayey aggregates forms around water drops. For water contents higher than 1.5 w_L, aggregates in samples prepared by S2 and S3 start to dilute, and all samples become qualitatively the same at the macroscale.

The results confirm that the final mean water content of 1.5 w_L has to be considered to ensure homogeneity of water content and particle arrangement for S1, as previous studies suggested [13, 15, 19, 59, 60]; however, the water content should be higher than 1.5 w_L for S2 and S3 due to the presence of aggregates at the macroscale.

5.2. Effect of Sand Geometry on Clay Location in Sand-Clay Mixtures. In the three types of samples, K Clay is present as a clay matrix around sandy particles and as a discontinuous micrometer layer around the sand in humid and dry samples. This discontinuous clay layer is possibly caused by several effects of (a) the shape of sand particles, which while rotating, bring about clay particles to spread on their surface; (b) the heterogeneous roughness of sand particles: sand cavities capture clay particles during their rotation [93, 94], and (c) the desiccation process at 105°C: the viscous clay matrix shrinks while surrounding the grains [56].

Angular edges of sandy grains are clay-poor, showing that clay covert is mainly due to a geometric effect on the sand surface, which is emphasized by desiccation [95]. Clays are caught on the sand for an interval of roughness which is dependent on particle size [96]. A minimum roughness is required to catch clays on sand surface and above a maximum roughness, clays cannot be stocked [97]. At dry state, angular edges are then preferential contact points or contact surfaces between sandy grains.

5.3. Effect of Drying on the Multiscale Structure of Sand-Clay Mixtures. The desiccation process caused clay matrix shrinkage and crack opening within the matrix and at the interface between clay matrix and sandy grains. For water contents lower than 1.5 w_L, the desiccation of the matrix showed different patterns under SEM. Clay matrix exists as a more continuous phase and shows fewer cracks in S1 than S2 and S3 samples due to less shrinkage occurred in S1 samples (see Figure 5).

For dry samples initially mixed at water contents higher than 1.5 w_L, aggregates are not clearly visible at the mesoscale under X-ray tomography, SEM, or ESEM, contrary to the macroscale. As a consequence, the desiccation process has probably caused a rearrangement of clayey particles, which formed aggregates [98], as the microstructure of clay material can be significantly affected by drying methods [61].

5.4. Effect of Sample Preparation on the Porosity. At the mesoscale under X-ray tomography, all samples have similar pore size distribution (connected or not) but slightly different mean porosities, which highlights that the number of macropores, but not their size, varies as a function of the sample. Different macropore size distributions were detected by MIP tests, which is interpreted by different pore connectivity because of varying size and density of desiccation cracks [88].

At the meso- and microscales, S2 and S3 have the same mean pore size distribution contrary to S1, which is characterized by larger mesopores. In clay soils and clay rocks

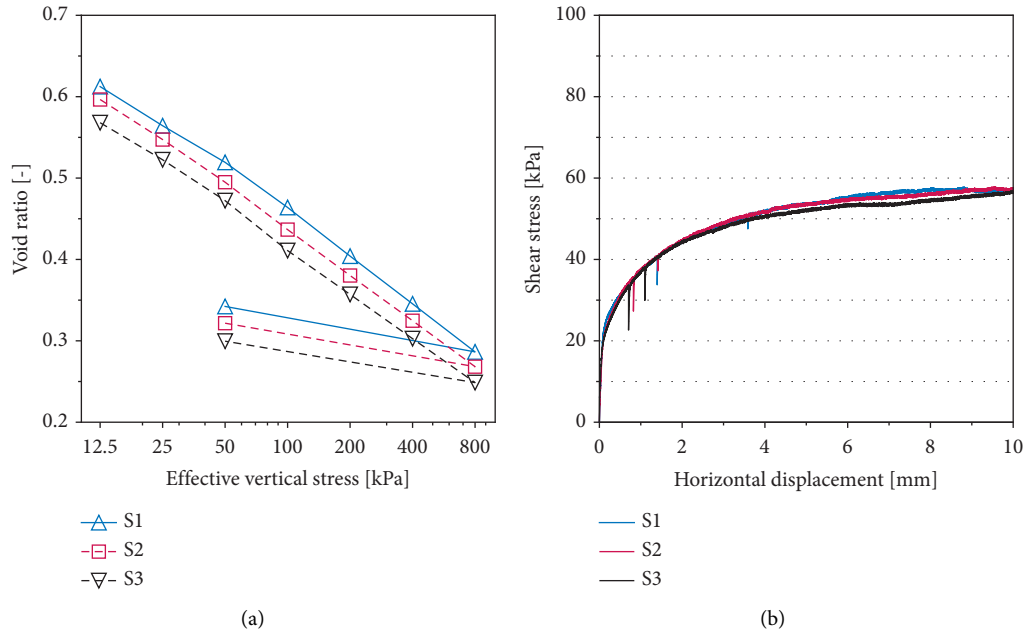

Figure 10: Mechanical behavior of the three sample preparations S1, S2, and S3 in (a) oedometer test and (b) direct shear test.

[95, 99], mesopores usually separate clay minerals organized in flakes that contain interlayered and bound water. The larger size of mesopores in S1 is interpreted by a more efficient dispersion of kaolinite in water in comparison to S2 and S3.

The mean porosity (including macro- to microporosity) values of all samples reveal that on average, porosity differences do not exceed 5% among the different sample preparations. However, even if the mean porosity is close, different fractions of micro-, meso-, and macropores are highlighted. In conclusion, samples prepared by S1 contain a lower fraction of larger mesopores and a significantly smaller median pore size, which confirms that clay minerals are better dispersed in the mixtures prepared by S1 than S2 and S3.

6. Conclusion

Regarding the high number of experimental studies involving variable preparations of clay soil samples, mixtures of Fontainebleau sand, K Clay, and water were prepared by three different protocols to investigate the effect of the sample preparation on their texture. From centimeters to micrometers, different imaging and bulk techniques were used to perform the comparison between the three protocols: optical photography, 3D X-ray tomography, SEM, ESEM, and MIP.

The study reveals that the protocol, which consists of mixing sand firstly, then water, and lastly clays, allows preparing samples with a better dispersion of clays with no significant macroscopic clayey aggregates. The samples prepared in this way contain, on average, a lower mean porosity with a lower mean and median pore size, despite of larger mesopores but in lower quantity than in the other preparations. The repeatable mechanical behavior from oedometer and direct shear tests reveals that the sample heterogeneities of the three preparations are limited and not so significant, for what concerns the macroscopic mechanical response. For a better dispersion of mineral phases within the samples, S1 preparation is, therefore, more recommended for engineering applications that require homogeneous clayey soil samples.

The rheological response of artificial soils can be significantly altered by the identified varying pore distributions. Future studies should therefore examine such differences when developing geomechanical tests other than the considered oedometric and shear ones. The effect of the sample preparation should be investigated on different weight fractions of sand and clay as well.

Data Availability

The quantitative results from MIP and X-ray tomography are available online on the Mendeley data set at https://data.mendeley.com/datasets/6vbyfyhd7y/1 (DOI: https://doi.org/10.17632/6vbyfyhd7y.1). The porosimetry raw data (pore diameter vs. pore pressure and cumulative intrusion curves vs. pore diameter) and the raw sets of 8 bit-images of S1, S2, and S3 samples (0–100 images per sample) are shared.

Conflicts of Interest

The authors declare that they have no conflicts of interest. All the data generated or analyzed during this study are included in this published article and its supplementary information files.

Acknowledgments

The authors would like to express their acknowledgment to M. Yannick Benoit, M. Francois Bertrand, Pr. Emmanuel

Roziere, and M. Mathias Marcel for their technical assistance.

References

[1] A. Gens, L. d. N. Guimaraes, A. Garcia-Molina, and E. Alonso, "Factors controlling rock-clay buffer interaction in a radioactive waste repository," *Engineering Geology*, vol. 64, no. 2-3, pp. 297–308, 2002.

[2] R. R. Shakir and J. Zhu, "Behavior of compacted clay-concrete interface," *Frontiers of Architecture and Civil Engineering in China*, vol. 3, no. 1, pp. 85–92, 2009.

[3] F. Dupray, B. François, and L. Laloui, "Analysis of the FEBEX multi-barrier system including thermoplasticity of unsaturated bentonite," *International Journal for Numerical and Analytical Methods in Geomechanics*, vol. 37, no. 4, pp. 399–422, 2013.

[4] Y. Abed, D. A. Bouzid, S. Bhattacharya, and M. H. Aissa, "Static impedance functions for monopiles supporting offshore wind turbines in nonhomogeneous soils-emphasis on soil/monopile interface characteristics," *Earthquakes and Structures*, vol. 10, no. 5, pp. 1143–1179, 2016.

[5] A. Di Donna, A. Ferrari, and L. Laloui, "Experimental investigations of the soil-concrete interface: physical mechanisms, cyclic mobilization, and behaviour at different temperatures," *Canadian Geotechnical Journal*, vol. 53, no. 4, pp. 659–672, 2016.

[6] A. R. Vasilescu, A.-L. Fauchille, C. Dano, P. Kotronis, R. Manirakiza, and P. Gotteland, "Impact of temperature cycles at soil-concrete interface for energy piles," in *International Symposium on Energy Geotechnics, Springer Series in Geomechanics and Geoengineering*, pp. 35–42, Springer, Berlin, Germany, 2018.

[7] R. Vasilescu, K. Yin, A.-L. Fauchille et al., "Influence of thermal cycles on the deformation of soil-pile interface in energy piles," in *Proceedings of the E3S Web of Conferences*, vol. 92, p. 13004, June 2019.

[8] A. K. Howard, "The revised ASTM standard on the unified classification system," *Geotechnical Testing Journal*, vol. 7, no. 4, pp. 216–222, 1984.

[9] ASTM-D2487, *Classification of Soils for Engineering Purposes (Unified Soil Classification System)*, American Society for Testing Materials, Philadelphia, PA, USA, 1992.

[10] M. A. Dafalla, "Effects of clay and moisture content on direct shear tests for clay-sand mixtures," *Advances in Materials Science and Engineering*, vol. 2013, Article ID 562726, 2013.

[11] D. Tessier, "Behaviour and microstructure of clay minerals,"in *Soil Colloids and Their Associations in Aggregates*, NATO ASI Series, pp. 387–415, Springer, Berlin, Germany, 1990.

[12] M. Al-Mukhtar, N. Belanteur, D. Tessier, and S. Vanapalli, "The fabric of a clay soil under controlled mechanical and hydraulic stress states," *Applied Clay Science*, vol. 11, no. 2-4, pp. 99–115, 1996.

[13] D. Muir Wood and G. V. Kumar, "Experimental observations of behaviour of heterogeneous soils," *Mechanics of Cohesive-Frictional Materials*, vol. 5, no. 5, pp. 373–398, 2000.

[14] S. Thevanayagam, T. Shenthan, S. Mohan, and J. Liang, "Undrained fragility of clean sands, silty sands, and sandy silts," *Journal of Geotechnical and Geoenvironmental Engineering*, vol. 128, no. 10, pp. 849–859, 2002.

[15] N. Yavari, A. M. Tang, J.-M. Pereira, and G. Hassen, "Effect of temperature on the shear strength of soils and the soil-structure interface," *Canadian Geotechnical Journal*, vol. 53, no. 7, pp. 1186–1194, 2016.

[16] R. Kuerbis and Y. P. Vaid, "Sand sample preparation-the slurry deposition method," *Soils and Foundations*, vol. 28, no. 4, pp. 107–118, 1988.

[17] J. A. H. Carraro and M. Prezzi, "A new slurry-based method of preparation of specimens of sand containing fines," *Geotechnical Testing Journal*, vol. 31, no. 1, pp. 1–11, 2008.

[18] K. Yin, J. Liu, J. Lin, A.-R. Vasilescu, K. Othmani, and E. Di Filippo, "Interface direct shear tests on JEZ-1 mars regolith simulant," *Applied Sciences*, vol. 11, no. 15, p. 7052, 2021.

[19] G. V. Kumar and D. M. Wood, "Mechanical behaviour of mixtures of kaolin and coarse sand," in *Proceedings of the IUTAM Symposium on Mechanics of Granular and Porous Materials*, pp. 57–68, Springer, Cambridge, UK, July 1997.

[20] G. V. Kumar and D. M. Wood, "Fall cone and compression tests on clay ± gravel mixtures," *Géotechnique*, vol. 49, no. 6, pp. 727–739, 1999.

[21] L. E. Vallejo and R. Mawby, "Porosity influence on the shear strength of granular material-clay mixtures," *Engineering Geology*, vol. 58, no. 2, pp. 125–136, 2000.

[22] A. F. Cabalar and R. A. Hasan, "Compressional behaviour of various size/shape sand-clay mixtures with different pore fluids," *Engineering Geology*, vol. 164, pp. 36–49, 2013.

[23] Y. Deng, Z. Wu, Y. Cui, S. Liu, and Q. Wang, "Sand fraction effect on hydro-mechanical behavior of sand-clay mixture," *Applied Clay Science*, vol. 135, pp. 355–361, 2017.

[24] U.-G. Kim, L. Zhuang, D. Kim, and J. Lee, "Evaluation of cyclic shear strength of mixtures with sand and different types of fines," *Marine Georesources & Geotechnology*, vol. 35, no. 4, pp. 447–455, 2017.

[25] N. Zhang, X. Yu, A. Pradhan, and A. J. Puppala, "A new generalized soil thermal conductivity model for sand-kaolin clay mixtures using thermo-time domain reflectometry probe test," *Acta Geotechnica*, vol. 12, no. 4, pp. 739–752, 2017.

[26] D. Kim, B. H. Nam, and H. Youn, "Effect of clay content on the shear strength of clay-sand mixture," *International Journal of Geo-Engineering*, vol. 9, no. 1, p. 19, 2018.

[27] K. Yin, A.-L. Fauchille, K. Othmani et al., "Influence of sample preparation on the multi scale structure of sand-clay mixtures," in *Proceedings of the E3S Web of Conferences*, vol. 92, p. 01007, June 2019.

[28] P. Delage, "A microstructure approach to the sensitivity and compressibility of some Eastern Canada sensitive clays," *Géotechnique*, vol. 60, no. 5, pp. 353–368, 2010.

[29] R. Bennett and M. Hulbert, *Clay Microstructure*, Springer Science & Business Media, Berlin, Germany, 2012.

[30] Y. T. Kiki, N. Saiyouri, V. Gbaguidi, Y. Anguy, C. Gaborieau, and R. Fabre, "Microstructural, chemical and mineralogical analyses for understanding the geotechnical properties of clayey soils," *Journal of Minerals and Materials Characterization and Engineering*, vol. 4, no. 6, pp. 305–319, 2016.

[31] N. Ural, "The importance of clay in geotechnical engineering," in *Current Topics in the Utilization of Clay in Industrial and Medical Applications*, M. Zoveidavianpoor, Ed., IntechOpen, London, UK, 2018.

[32] E. A. Miller and G. F. Sowers, "The strength characteristics of soil-aggregate mixtures & discussion," *Highway Research Board Bulletin*, vol. 183, pp. 16–32, 1958.

[33] S. Thevanayagam and S. Mohan, "Intergranular state variables and stress-strain behaviour of silty sands," *Géotechnique*, vol. 50, no. 1, pp. 1–23, 2000.

[34] A. Revil, D. Grauls, and O. Brévart, "Mechanical compaction of sand/clay mixtures," *Journal of Geophysical Research: Solid Earth*, vol. 107, no. B11, pp. ECV 11-11–ECV 11-15, 2002.

[35] X. Wei, M. Hattab, J.-M. Fleureau, and R. Hu, "Micro-macro-experimental study of two clayey materials on drying paths," *Bulletin of Engineering Geology and the Environment*, vol. 72, no. 3-4, pp. 495–508, 2013.

[36] L. Zuo and B. A. Baudet, "Determination of the transitional fines content of sand-non plastic fines mixtures," *Soils and Foundations*, vol. 55, no. 1, pp. 213–219, 2015.

[37] M. Emiroğlu, A. Yalama, and Y. Erdoğdu, "Performance of ready-mixed clay plasters produced with different clay/sand ratios," *Applied Clay Science*, vol. 115, pp. 221–229, 2015.

[38] E. Polidori, "Relationship between the Atterberg limits and clay content," *Soils and Foundations*, vol. 47, no. 5, pp. 887–896, 2007.

[39] F. Bendahmane, D. Marot, and A. Alexis, "Experimental parametric study of suffusion and backward erosion," *Journal of Geotechnical and Geoenvironmental Engineering*, vol. 134, no. 1, pp. 57–67, 2008.

[40] D. Marot, F. Bendahmane, F. Rosquoët, and A. Alexis, "Internal flow effects on isotropic confined sand-clay mixtures," *Soil and Sediment Contamination: International Journal*, vol. 18, no. 3, pp. 294–306, 2009.

[41] A. F. Cabalar and W. S. Mustafa, "Fall cone tests on clay-sand mixtures," *Engineering Geology*, vol. 192, pp. 154–165, 2015.

[42] T. Kanit, S. Forest, I. Galliet, V. Mounoury, and D. Jeulin, "Determination of the size of the representative volume element for random composites: statistical and numerical approach," *International Journal of Solids and Structures*, vol. 40, no. 13-14, pp. 3647–3679, 2003.

[43] S. Torquato and H. Haslach Jr., "Random heterogeneous materials: microstructure and macroscopic properties," *Applied Mechanics Reviews*, vol. 55, no. 4, pp. B62–B63, 2002.

[44] M. D. Bolton, M. W. Gui, J. Garnier et al., "Centrifuge cone penetration tests in sand," *Géotechnique*, vol. 49, no. 4, pp. 543–552, 1999.

[45] C. Gaudin, F. Schnaid, and J. Garnier, "Sand characterization by combined centrifuge and laboratory tests," *International Journal of Physical Modelling in Geotechnics*, vol. 5, no. 1, pp. 42–56, 2005.

[46] S. Pra-Ai, "Behaviour of soil-structure interfaces subjected to a large number of cycles. application to piles," Ph. D. thesis, Univ. of Grenoble, Grenoble, France, 2013.

[47] S. Pra-ai and M. Boulon, "Soil-structure cyclic direct shear tests: a new interpretation of the direct shear experiment and its application to a series of cyclic tests," *Acta Geotechnica*, vol. 12, no. 1, pp. 107–127, 2017.

[48] A.-R. Vasilescu, *Design and Execution of Energy Piles: Validation by In-Situ and Laboratory Experiments*, École Centrale de Nantes, Nantes, France, 2019.

[49] K. Yin, J. Liu, A.-R. Vasilescu, E. Di Filippo, and K. Othmani, "A procedure to prepare sand-clay mixture samples for soil-structure interface direct shear tests," *Applied Sciences*, vol. 11, no. 12, p. 5337, 2021.

[50] T. Hammad, *Comportement Des Sédiments Marins De Grande Profondeur: Approche Multiéchelle*, Ecole Centrale de Paris, Châtenay-Malabry, France, 2010.

[51] R. San Nicolas, M. Cyr, and G. Escadeillas, "Characteristics and applications of flash metakaolins," *Applied Clay Science*, vol. 83-84, pp. 253–262, 2013.

[52] A. Martinez and H. H. Stutz, "Rate effects on the interface shear behaviour of normally and overconsolidated clay," *Géotechnique*, vol. 69, no. 9, pp. 801–815, 2019.

[53] A. Aboulayt, R. Jaafri, H. Samouh et al., "Stability of a new geopolymer grout: rheological and mechanical performances of metakaolin-fly ash binary mixtures," *Construction and Building Materials*, vol. 181, pp. 420–436, 2018.

[54] M. Hattab and J.-M. Fleureau, "Experimental study of kaolin particle orientation mechanism," *Géotechnique*, vol. 60, no. 5, pp. 323–331, 2010.

[55] A. Ben Hassine, H. Souli, P. H. Dubujet, F. Ayari, and M. Trabelsi-Ayadi, "Kaolinite carbonate mixture fabric evolution after electrokinetic tests," *Géotechnique Letters*, vol. 6, no. 1, pp. 45–49, 2016.

[56] B. A. Albrecht and C. H. Benson, "Effect of desiccation on compacted natural clays," *Journal of Geotechnical and Geoenvironmental Engineering*, vol. 127, no. 1, pp. 67–75, 2001.

[57] N. O. Abdulhadi, *An Experimental Investigation into the Stress-dependent Mechanical Behavior of Cohesive Soil with Application to Wellbore Instability*, Massachusetts Institute of Technology, Cambridge, MA, USA, 2009.

[58] J. C. Robinet, P. Sardini, D. Coelho et al., "Effects of mineral distribution at mesoscopic scale on solute diffusion in a clay-rich rock: example of the Callovo-Oxfordian mudstone (Bure, France)," *Water Resources Research*, vol. 48, no. 5, 2012.

[59] T. Hammad, J.-M. Fleureau, and M. Hattab, "Kaolin/montmorillonite mixtures behaviour on oedometric path and microstructural variations," *European Journal of Environmental and Civil Engineering*, vol. 17, no. 9, pp. 826–840, 2013.

[60] M. Hattab, T. Hammad, and J.-M. Fleureau, "Internal friction angle variation in a kaolin/montmorillonite clay mix and microstructural identification," *Géotechnique*, vol. 65, no. 1, pp. 1–11, 2015.

[61] M. E. Houben, G. Desbois, and J. L. Urai, "A comparative study of representative 2D microstructures in Shaly and Sandy facies of opalinus clay (Mont Terri, Switzerland) inferred form BIB-SEM and MIP methods," *Marine and Petroleum Geology*, vol. 49, pp. 143–161, 2014.

[62] P. Y. Hicher, H. Wahyudi, and D. Tessier, "Microstructural analysis of inherent and induced anisotropy in clay," *Mechanics of Cohesive-Frictional Materials*, vol. 5, no. 5, pp. 341–371, 2000.

[63] M. Hattab and J.-M. Fleureau, "Experimental analysis of kaolinite particle orientation during triaxial path," *International Journal for Numerical and Analytical Methods in Geomechanics*, vol. 35, no. 8, pp. 947–968, 2011.

[64] A. L. Fauchille, A. P. van den Eijnden, L. Ma et al., "Variability in spatial distribution of mineral phases in the Lower Bowland Shale, UK, from the mm- to μm-scale: quantitative characterization and modelling," *Marine and Petroleum Geology*, vol. 92, pp. 109–127, 2018.

[65] A.-L. Fauchille, S. Hedan, V. Valle, D. Pret, J. Cabrera, and P. Cosenza, "Relationships between cracking, strains and proportions of clay matrix and rigid inclusions in Tournemire clay rock," in *Proceedings of the 2nd Petrus-OPERA PhD and Early Stage Researcher Conference 2016*, p. 42, Netherlands, July 2016.

[66] M. Houben, B. Laurich, G. Desbois, and J. Urai, "Microstructure and porosity of opalinus clay at the Mont Terri rock laboratory (Switzerland)," in *Proceedings of the EGU General Assembly Conference Abstracts*, p. 2651, Vienna, Austria, April 2012.

[67] G. D. Danilatos, "Introduction to the ESEM instrument," *Microscopy Research and Technique*, vol. 25, no. 5-6, pp. 354–361, 1993.

[68] A. Sufian and A. R. Russell, "Microstructural pore changes and energy dissipation in Gosford sandstone during pre-failure loading using X-ray CT," *International Journal of Rock Mechanics and Mining Sciences*, vol. 57, pp. 119–131, 2013.

[69] T. Meier, E. Rybacki, T. Backers, and G. Dresen, "Influence of bedding angle on borehole stability: a laboratory investigation of transverse isotropic oil shale," *Rock Mechanics and Rock Engineering*, vol. 48, no. 4, pp. 1535–1546, 2015.

[70] G. Viggiani, E. Andò, D. Takano, and J. Santamarina, "Laboratory X-ray tomography: a valuable experimental tool for revealing processes in soils," *Geotechnical Testing Journal*, vol. 38, no. 1, pp. 61–71, 2015.

[71] M. Cała, K. Cyran, A. Stopkowicz, M. Kolano, and M. Szczygielski, "Preliminary application of X-ray computed tomograph on characterisation of polish gas shale mechanical properties," *Rock Mechanics and Rock Engineering*, vol. 49, no. 12, pp. 4935–4943, 2016.

[72] F. Figueroa Pilz, *4D strain quantification during maturation 5 of kimmeridge clay using synchrotron X-ay tomography*, Thesis, The University of Manchester, Manchester, UK, 2016.

[73] L. Ma, K. G. Taylor, P. J. Dowey, L. Courtois, A. Gholinia, and P. D. Lee, "Multiscale 3D characterisation of porosity and organic matter in shales with variable TOC content and thermal maturity: examples from the Lublin and Baltic Basins, Poland and Lithuania," *International Journal of Coal Geology*, vol. 180, pp. 100–112, 2017.

[74] E. Stavropoulou, E. Andò, E. Roubin et al., "Dynamics of water absorption in Callovo-Oxfordian claystone revealed with multimodal x-ray and neutron tomography," *Frontiers of Earth Science*, vol. 8, p. 6, 2020.

[75] T. Kozaki, S. Suzuki, N. Kozai, S. Sato, and H. Ohashi, "Observation of microstructures of compacted bentonite by microfocus X-ray computerized tomography (Micro-CT)," *Journal of Nuclear Science and Technology*, vol. 38, no. 8, pp. 697–699, 2001.

[76] M. Van Geet, G. Volckaert, and S. Roels, "The use of microfocus X-ray computed tomography in characterising the hydration of a clay pellet/powder mixture," *Applied Clay Science*, vol. 29, no. 2, pp. 73–87, 2005.

[77] C. Kawaragi, T. Yoneda, T. Sato, and K. Kaneko, "Saturated structures," *Saturated Model Theory*, vol. 106, no. 1-2, pp. 51–57, 2009.

[78] L. Ma, K. G. Taylor, P. D. Lee, K. J. Dobson, P. J. Dowey, and L. Courtois, "Novel 3D centimetre-to nano-scale quantification of an organic-rich mudstone: the carboniferous Bowland Shale, Northern England," *Marine and Petroleum Geology*, vol. 72, pp. 193–205, 2016.

[79] D. Prêt, S. Sammartino, D. Beaufort et al., "A new method for quantitative petrography based on image processing of chemical element maps: part II. Semi-quantitative porosity maps superimposed on mineral maps," *American Mineralogist*, vol. 95, no. 10, pp. 1389–1398, 2010.

[80] S. Diamond, "Pore size distributions in clays," *Clays and Clay Minerals*, vol. 18, no. 1, pp. 7–23, 1970.

[81] S. Diamond, "Microstructure and pore structure of impact-compacted clays," *Clays and Clay Minerals*, vol. 19, no. 4, pp. 239–249, 1971.

[82] D. Penumadu and J. Dean, "Compressibility effect in evaluating the pore-size distribution of kaolin clay using mercury intrusion porosimetry," *Canadian Geotechnical Journal*, vol. 37, no. 2, pp. 393–405, 2000.

[83] H. Zhou, Y.-g. Fang, R.-g. Gu, and C. Zeng, "Microscopic analysis of saturated soft clay in pearl river delta," *Journal of Central South University*, vol. 18, no. 2, pp. 504–510, 2011.

[84] E. W. Washburn, "The dynamics of capillary flow," *Physical Review*, vol. 17, no. 3, pp. 273–283, 1921.

[85] S. Diamond, "Mercury porosimetry," *Cement and Concrete Research*, vol. 30, no. 10, pp. 1517–1525, 2000.

[86] ASTM D3080 / D3080M-11, *Standard Test Method for Direct Shear Test of Soils Under Consolidated Drained Conditions (Withdrawn 2020)*, ASTM International, West Conshohocken, PA, USA, 2011, https://www.astm.org.

[87] J. Rouquerol, D. Avnir, C. W. Fairbridge et al., "Recommendations for the characterization of porous solids (technical report)," *Pure and Applied Chemistry*, vol. 66, no. 8, pp. 1739–1758, 1994.

[88] J. Kodikara, S. Barbour, and D. Fredlund, "Changes in clay structure and behaviour due to wetting and drying," in *Proceedings of the 8th Australia New Zealand Conference on Geomechanics: Consolidating Knowledge*, p. 179, Australian Geomechanics Society, Hobart, Australia, February 1999.

[89] G. Jozefaciuk, T. Toth, and G. Szendrei, "Surface and micropore properties of saline soil profiles," *Geoderma*, vol. 135, pp. 1–15, 2006.

[90] R. A. Schoonheydt and C. T. Johnston, "Surface and interface chemistry of clay minerals," in *Developments in clay Science*, pp. 139–172, Elsevier, Amsterdam, Netherlands, 2013.

[91] W. J. Likos and N. Lu, "A laser technique to quantify the size, porosity, and density of clay clusters during sedimentation," *Geotechnical Testing Journal*, vol. 24, no. 1, pp. 83–91, 2001.

[92] C. J. Biermann, *Handbook of Pulping and Papermaking*, Elsevier, Amsterdam, Netherlands, 1996.

[93] M. Krasowska, R. Krastev, M. Rogalski, and K. Malysa, "Air-facilitated three-phase contact formation at hydrophobic solid surfaces under dynamic conditions," *Langmuir*, vol. 23, no. 2, pp. 549–557, 2007.

[94] D. I. Verrelli, W. J. Bruckard, P. Koh, M. Schwarz, and B. Follink, "Influence of particle shape and roughness on the induction period for particle-bubble attachment," in *Proceedings of the 26th International Mineral Processing Congress (IMPC-XXVI)*, pp. 24–28, New Delhi, India, September 2012.

[95] A. Meunier, *Clays*, Springer Science & Business Media, Berlin, Germany, 2005.

[96] J. Katainen, M. Paajanen, E. Ahtola, V. Pore, and J. Lahtinen, "Adhesion as an interplay between particle size and surface roughness," *Journal of Colloid and Interface Science*, vol. 304, no. 2, pp. 524–529, 2006.

[97] J. Jerez, M. Flury, J. Shang, and Y. Deng, "Coating of silica sand with aluminosilicate clay," *Journal of Colloid and Interface Science*, vol. 294, no. 1, pp. 155–164, 2006.

[98] L. A. Douglas, *Soil Micromorphology: A Basic and Applied Science*, Elsevier, Amsterdam, Netherlands, 1990.

[99] B. Yven, S. Sammartino, Y. Geraud, F. Homand, and F. Villieras, "Mineralogy, texture and porosity of callovo-oxfordian argillites of the meuse/haute-marne region (eastern Paris Basin)," *Mémoires de la Société géologique de France*, vol. 178, no. 1, pp. 73–90, 2007.